공학석사학위논문

유연 생체전자기기 제작을 위한 통기성 섬유 기판 기반 금속 나노와이어 패터닝 연구

Metal Nanowire Patterning on Breathable Fiber-based Substrate for Flexible Bioelectronics Fabrication

2023 년 8 월

서울대학교 대학원

기계공학부

윤 혁 준

유연 생체전자기기 제작을 위한 통기성 섬유 기판 기반 금속 나노와이어 패터닝 연구

Metal Nanowire Patterning on Breathable Fiber-based Substrate for Flexible Bioelectronics Fabrication

지도교수 고 승 환

이 논문을 공학석사 학위논문으로 제출함

2023 년 4 월

서울대학교 대학원

기계공학부

윤 혁 준

윤 혁 준의 공학석사 학위논문을 인준함

2023 년 6 월

위 원 장 : 전 누 리 (인)

부위원장 : 고 승 환 (인)

위 원 : 신 용 대 (인)

Abstract

In this study, we have developed a process to efficiently fabricate flexible bioelectronics by rapidly and precisely patterning various conductive metal nanowires onto polymer fiber-based flexible substrates. The nanomaterials used in this process include Ag, Ag@Au, and Ag@(Au-Pt alloy) core-shell nanowires, which were synthesized and further enhanced in terms of mechanical and electrical stability through additional laser processing. Moreover, an insulating material can be printed as per the requirements to effectively implement desired functionalities. Utilizing this approach, we validated the performance of the developed process by creating heart-attachable epicardial signal recording bioelectronics, skin-attachable ascorbic acid (vitamin C) concentration measurement biosensors, and skin-attachable electromyography-based hand gesture recognition human-machine interfaces. The results demonstrate that the developed process can be effectively utilized for the fabrication of flexible bioelectronics.

Keyword : Flexible electronics, Bioelectronics, Nano-material patterning, Nano-material synthesis, Wearable electronics

Student Number : 2021-24389

Table of contents

Chapter 1. Introduction 1

1.1 Study backgrounds 1

1.2 Purpose of this research 1

Chapter 2. The nanowire selective filtration (NW-SF) 3

2.1 Principle of the NW-SF 3

2.2 Process optimization & Material characteristics 6

Chapter 3. Biocompatible characteristics & In vivo epicardial signal recording 9

3.1 Evaluation of biocompatibility 9

3.2 In vivo epicardial signal recording bioelectronics 10

Chapter 4. Non-enzymatic biosensor for ascorbic acid detection 14

4.1 Fabrication of the non-enzymatic biosensor 14

4.2 Electrochemical analysis for ascorbic acid detection 14

Chapter 5. Customized Human-Machine Interfaces (HMI) 18

5.1 Importance of the customized bioelectronics fabrication 18

5.2 Hand gesture classification with deep learning approach 20

Chapter 6. Conclusion 22

Chapter 7. Method 23

7.1 Materials 23

7.2 Synthesis of Ag nanowire 23

7.3 Synthesis of Ag@Au core-shell nanowire 24

7.4 Synthesis of Ag@(Au-Pt) core-shell nanowire 24

7.5 Material characterizations.....25

7.6 Laser specification.....25

7.7 Electrochemical analysis 26

7.8 Electromyography (EMG) signal acquisition circuit.....26

Reference 28

Abstract in Korean 30

List of figures

Figure 1. The schematic diagram of the nanowire selective filtration (NW-SF) process.

Figure 2. The schematic diagram of the (a) enlarged view of NW-SF process and (b) the comparison of the results between NW-SF on glass (blocked surface) and carbon paper (CP, porous surface). An example of (c) conformal epidermal electronics fabricated by NW-SF attached on a finger and (d) bioelectronics manufactured through roll-to-roll NW-SF process.

Figure 3. Process parameter & Material characteristics analysis (a) Scanning electron microscopy (SEM) image, (b) printing linewidth test (n=3), and (c) sheet resistance test after the dispenser printing of nanowire (n=3). (d) SEM image, (e) strain-resistance test under laser power variables, and (f) cycle test under 30% strain for 10,000 cycles after the laser scanning process. (g) Fourier-transform infrared spectroscopy (FT-IR) spectra of polyvonylpyrrolidone (PVP), Ag@Au NW, and Ag@(Au-Pt) NW, (h) breathability comparison of various membranes popular for epidermal electronics, and (i) mechanical modulus tests under strain up to 300%. The syringe with diameter of 4.71 mm was utilized in NW-SF for dispenser printing.

Figure 4. The result of (a) the cell viability test (n=3), and (b) the inductively coupled plasma-mass-spectrometry (ICP-MS) Ag ion leaching test under hydrogen peroxide of the nanomaterial used for the biocompatibility test.

Figure 5. (a) The impedance and phase angle spectra of the in vivo epicardial signal recording bioelectronics, and (b) the variance of the impedance under mechanical strains up to 30% (n=3).

Figure 6. (a) The schematic diagram of the epicardial signal recording with the

bioelectronics fabricated through NW-SF, (b) the enlarged image of the epicardial signal recording, (c) the result of the epicardial signal recording from a healty rat and a rat with myocardial infarction, and (d) the comparison of the inter-pulse-interval between a rat with (w/) and without (w/o) myocardial infarction. (n=3)

Figure 7. (a) The schematic image of a printed three-electrode biosensor and (b) skin-attached printed biosensor composed of three different sorts of nanowires fabricated by NW-SF. (c) Energy-dispersive X-ray spectroscopy (EDS) cross-sectional line scan plot and (d) mapping image of Ag@(Au-Pt) NW from transmission electron microscopy (TEM).

Figure 8. (a) The schematic image of the three-electrode biosensing principle, (b) cyclic voltammetry plot comparing cases w/ and w/o ascorbic acid in phosphate buffered saline (PBS) electrolyte, (c) sensitivity plot of printed biosensor with ascorbic acid concentration variation and (d) selectivity plot of printed biosensor with diverse components in body fluid.

Figure 9. (a) The schematic diagrams of the anatomical structure of the forearm (left arm) and (b) comparison of the electromyography signals from two subjects who are w/ and w/o their customized bioelectronics.

Figure 10. The schematic diagram of the overall structure of the hand gesture classification with customized human-machine interface (HMI) bioelectronics.

Figure 11. (a) The valid loss and the accuracy plot and (b) the confusion matrix of the result from the hand gesture classification with deep learning approach.

Chapter 1. Introduction

1.1. Study backgrounds

There has been extensive progress in the field of epidermal bioelectronics, which facilitated effective integration of the electronics with soft and dynamic human skin by virtue of their ultrathin, flexible and stretchable form factors[1]. Among various materials, electrospun polymer fiber-based membranes have gained huge attentions as substrate materials for epidermal bioelectronics on account of their flexible, breathable, and conformal attributes[2].

However, recent manufacturing processes of epidermal bioelectronics harnessing the electrospun polymer fiber-based substrates have some limitations in respect of the versatility and efficiency. For example, the most popular patterning method utilizing pre-designed mask[3] to pattern electrode materials has fundamental restrictions including difficulties of prompt design modification, and inevitable additional manufacturing process of mask fabrication. In addition, accompanying spray coating or stencil printing induce extensive waste of nanomaterials which have been recently considered as a serious environmental problem[4]. Moreover, conventional deposition methods need expensive vacuum facilities, and multi-material patterning in situ was limited with such conventional fabrication process, which require more time and manufacturing steps.

1.2. Purpose of this research

In this regard, this work proposes an efficient dispenser printing method for manufacturing epidermal bioelectronics on electrospun polymer fiber-based

membranes harnessing diverse metal nanowire inks. We were able to effectively print nanowires on the breathable polymer fiber-based substrate by allowing the solvent of the nanowire ink to flow down, yet leaving nanowires whose length is longer than the pore size of the membrane. During this process, the substrate was placed on porous carbon paper so that the solvent of the ink could be discharged effectively without vacuum facilities.

With its availability to conduct immediate design-production streak which is suitable for developing on-demand wearable electronics for various body-parts and human characteristics, in vivo epicardial recording on rodents' heart and surface-electromyography (EMG) on human skin were successfully conducted. Moreover, by virtue of the viability of patterning various sorts of nanowire inks in situ, a biosensor based on three-electrode system utilizing different nanomaterials for each electrode was effectively fabricated.

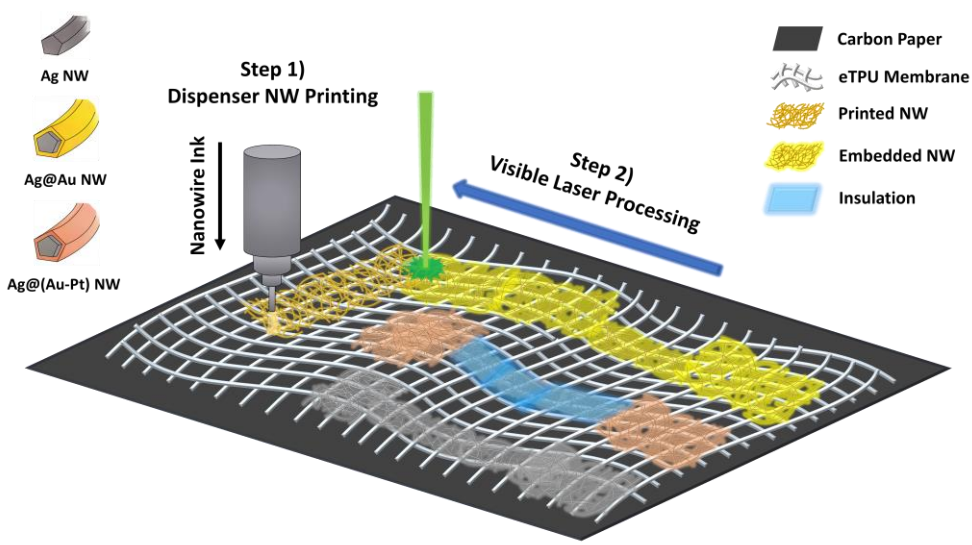

Figure 1. The schematic diagram of the nanowire selective filtration (NW-SF) process.

Chapter 2. The nanowire selective filtration (NW-SF)

2.1. Principle of the NW-SF

Figure 1 shows the overall production process of printed circuit on electrospun membrane using nanowire selective-filtration (NW-SF). After placing electrospun thermoplastic polyurethane membrane (eTPU) on a porous carbon paper, metal nanowires dispersed in ethanol are ejected on the eTPU which filters out only the nanowires and make the solution pass through it. This study adopted silver nanowire (Ag NW), silver@gold core-shell nanowire (Ag@Au NW), and silver@(gold-platinum alloy) core-shell nanowire (Ag@(Au-Pt) NW) to utilize their own advantages depending on bespoke applications.

The printed nanowires are then subjected to laser treatment to enhance their electrical conductivity and mechanical stability through laser-welding of nanowire junctions and laser-embedding of nanowires into eTPU fibers, respectively. The polyvonylpyrrolidone (PVP) ligand that surrounds the metal nanowires forms hydrogen bonds with TPU under high temperature[3], enabling stable bonds between the nanowire layer and the eTPU substrate with laser embedding process.

For insulation, hexane-diluted Polydimethylsiloxane (PDMS) also can be printed on the nanowire patterns, while minimizing the blocked region that may degrade the mechanical softness and mass permeability through the membrane.

To achieve high resolution, the key requirement of this setup is the rapid removal of the suspension liquid. The carbon paper beneath the eTPU plays a similar role to a vacuum bed, efficiently absorbing and draining the solvent, thereby preventing the nanowire suspension from spreading over the eTPU surface (**Figure 2a**).

Nanowires dispensed on eTPU over glass (non-porous) substrate laterally spread, and the dried trace of nanowire suspension leaves variegated trail of nanowire with wide linewidth and low electric conductivity. On the other hand, the rapid drain by the carbon paper significantly narrow down the linewidth of the nanowire pattern and realize high electrical conductivity with same printing parameters (**Figure 2b**).

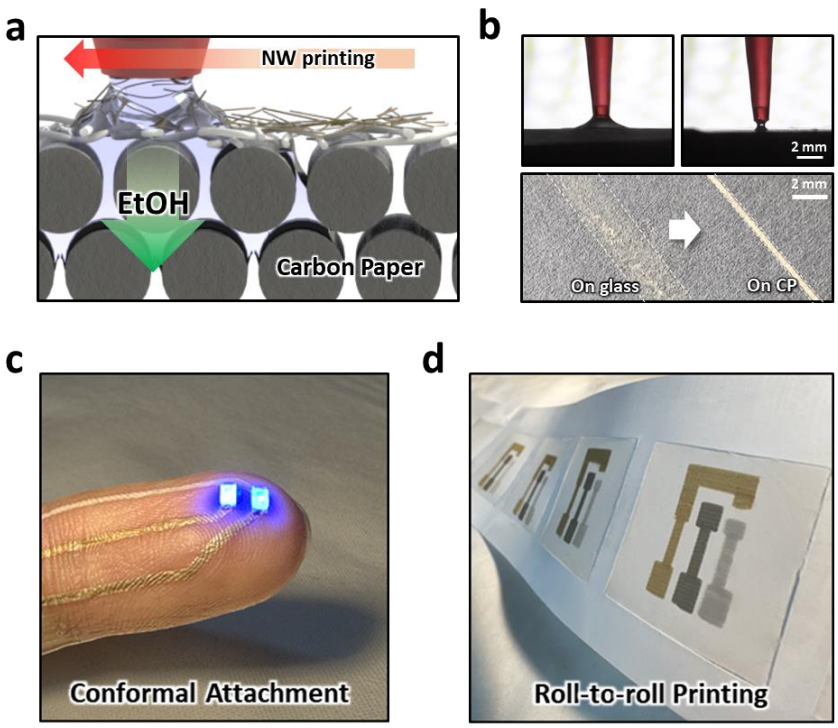

Figure 2. The schematic diagram of (a) the enlarged view of NW-SF process and (b) the comparison of the results between NW-SF on glass (non-porous surface) and carbon paper (CP, porous surface). An example of (c) conformal epidermal electronics fabricated by NW-SF attached on a finger and (d) bioelectronics manufactured through roll-to-roll NW-SF process.

The fabrication process minimally degrades the characteristics of the materials while supporting multi-nanowire applications, allowing the fabricated device to retain the functionalities of the composing materials, such as stertchability,

biocompatibility, and catalytic characteristics. Breathability test also reveals that, unlike Tagaderm or Polyimide (PI) which are commonly used substrates in bio-interfacing devices, eTPU/NW structure barely obstruct the flow of water vapor by virtue of its porous structure. When attaching the device to the living body for use, it can achieve high conformality (**Figure 2c**) by enhancing its wettability through oxygen (O_2) plasma treatment and subsequently employing the water wet-bonding technique. Consequently, NW-SF process offers the advantage of facile manufacturing equipment setup, making it also easily adaptable for a roll-to-roll manufacturing process as depicted in **Figure 2d**.

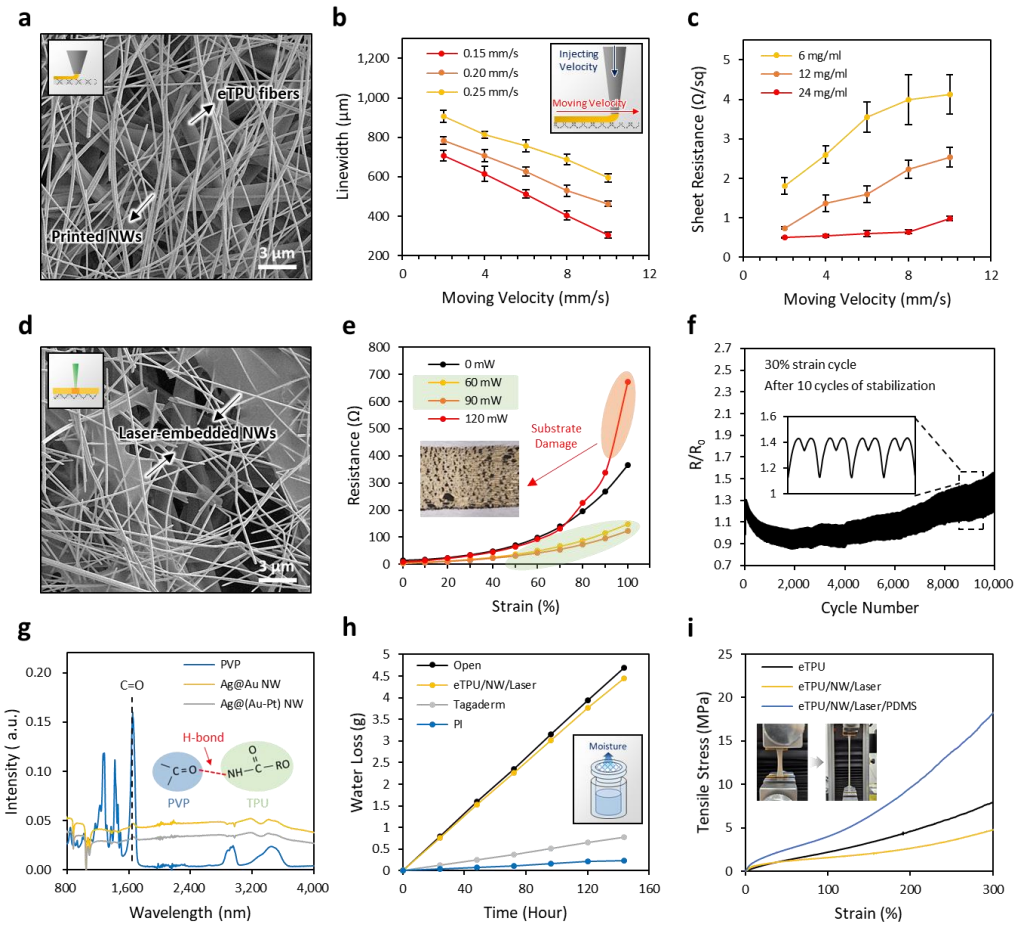

Figure 3. Process parameter & Material characteristics analysis (a) Scanning

electron microscopy (SEM) image, (b) printing linewidth test (n=3), and (c) sheet resistance test after the dispenser printing of nanowire (n=3). (d) SEM image, (e) strain-resistance test under laser power variables, and (f) cycle test under 30% strain for 10,000 cycles after the laser scanning process. (g) Fourier-transform infrared spectroscopy (FT-IR) spectra of polyvonylpyrrolidone (PVP), Ag@Au NW, and Ag@(Au-Pt) NW, (h) breathability comparison of various membranes popular for epidermal electronics, and (i) mechanical modulus tests under strain up to 300%. The syringe with diameter of 4.71 mm was utilized in NW-SF for dispenser printing.

2.2. Process optimization & Material characteristics

To achieve sufficient practical usability of both the fabrication process and the final output, a comprehensive examination and fine-tuning of the fabrication process were carried out, focusing on aspects such as pattern resolution, electric conductivity, mechanical stability, and insulation.

For the first step, we examined the effect of the moving speed, ejection rate on the linewidth, and the effect of the nanowire ink concentration on sheet resistance of the printed pattern. (**Figure 3b, 3c**). Overall, the linewidth tends to linearly decrease as moving speed increases and increase as the ejection rate increases. With the 25G taper nozzle, the minimum available linewidth is measured to be 300 um which is considered to be enough resolution to fabricate various flexible bioelectronics. In practical usage, high ejection rate modes are also expected to be effectively utilized for the cases where large area patterning is required. In **Figure 3c**, sheet resistance of printed Ag@Au NW region was investigated. The sheet resistance is proportional to the moving speed of the nozzle, while it is decreased with higher concentration of nanowire ink.

For the second step, the application of thermal treatment through laser

processing enhances the mechanical stability of the NW-eTPU structure, as shown in **Figure 3d**, where the nanowires are partially embedded in the eTPU. The laser energy absorbed by the nanowire is instantaneously converted into thermal energy, resulting in the shallow melting of the interfacing eTPU, and concurrently welding the nanowire junctions to increase the electrical conductivity of the nanowire network. In our experiments, we employed a 532 nm continuous laser as the power source with a scan speed of 40 mm/s. The 532 nm wavelength effectively matches the nanowire's laser absorption range, and the continuous power profile suppresses ablation phenomenon, ensuring consistent and uniform heat supply over the targeted area of the laser spot. **Figure 3e** illustrates the effect of laser power on the mechanical stability of the NW-eTPU structure, represented by the resistance change against strain. Notably, laser powers ranging from 60 mW to 90 mW significantly enhance the stability of the NW network against strain, while excessive power exacerbates it. We also confirmed that the sample laser treated with 90 mW had reliable electrical conductivity under cycling stress with 30% strain over 10,000 cycles (**Figure 3f**).

As a final stage of fabricating an electric circuit, we can also selectively insulate the printed electrode with polydimethylsiloxane (PDMS):hexane (4:1, weight/weight) using the same dispensing system. This study adopted PDMS as an insulating material, and the PDMS prepolymer was diluted with hexane by 80% to lower the viscosity during ejection through the nozzle. **Figure 3g** displays fourier-transform infrared spectroscopy (FT-IR) spectra of the PVP, Ag@Au NW, and Ag@(Au-Pt) NW. According to the previous study[3], PVP ligand of the Ag nanowire and Polyurethane (PU) form hydrogen bond between them, enabling enhanced robust attachment under thermal treatment. In the same regard, we could

ascertain that the synthesized Ag@Au NW and Ag@(Au-Pt) NW also have PVP ligands, which allow them to formulate hydrogen bonds. **Figure 3h** presents a breathability study for popular materials for epidermal electronics. According to the result, the membrane fabricated via NW-SF showed similar breathability compared with the case of no physical membrane. Mechanical modulus is an essential factor in soft-electronics as it significantly influences not only the safety of wearing, but also the conformal and reliable attachment of the device to the living organ. The study on tensile stress (**Figure 3i**) of three types of samples shows that the Young's modulus of the bare sample (eTPU) is about 1.66 MPa, and it slightly decreases after nanowire/laser treatment (eTPU/NW/Laser). Inevitably, PDMS insulation layer increases the Young's modulus up to 6.7 MPa, yet such figure is still fairly small value when it compared to the tensile modulus of skin or muscles[5].

Chapter 3. Biocompatible characteristics & In vivo epicardial signal recording

3.1. Evaluation of biocompatibility

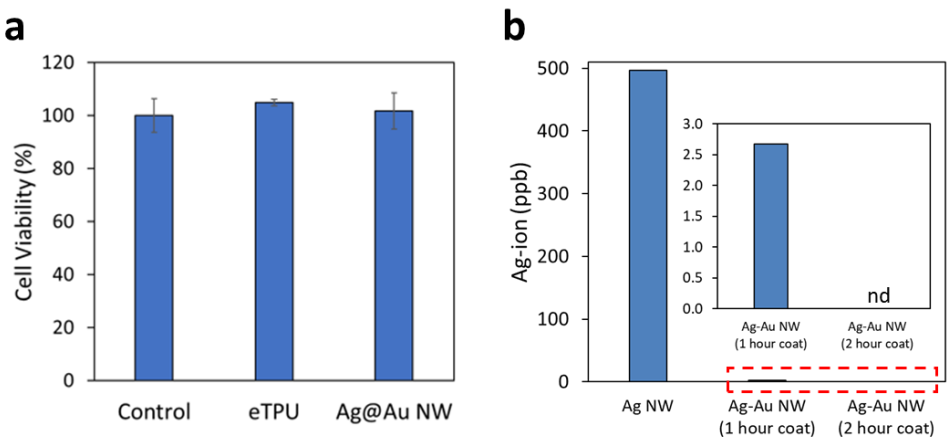

Figure 4. The result of (a) the cell viability test (n=3), and (b) the inductively coupled plasma-mass-spectrometry (ICP-MS) Ag ion leaching test under hydrogen peroxide of the nanomaterial used for the biocompatibility test.

In this chapter, we will discuss and evaluate the potential of the bioelectronics which can be produced through NW-SF. In addition to the mechanical and electrical characteristics analyzed above, we also tested the suitability of the fabricated bioelectronics as in vivo implantable applications. The biocompatibility test was conducted on eTPU membranes and Ag@Au NW composing in vivo electrodes.

By referring to the biocompatibility test of a previous research[6], we report that both the eTPU membrane substrate and the eTPU membrane with Ag@Au core-shell nanowires patterned through NW-SF exhibited high cell viability in cell

culture tests using L929 mouse fibroblast cells (**Figure 4a**). Moreover, to determine the extent of Ag ion release, which is known to be harmful to living organisms, we performed ICP-MS tests, revealing that the synthesized Ag@Au NW showed minimal Ag ion release (**Figure 4b**). Based on these results and considering the mechanical and electrical properties previously confirmed, the bioelectronics patterned by NW-SF with proper materials is deemed to possess high biocompatibility and holds potential as a novel medium for implantable bio applications.

3.2. In vivo epicardial signal recording bioelectronics

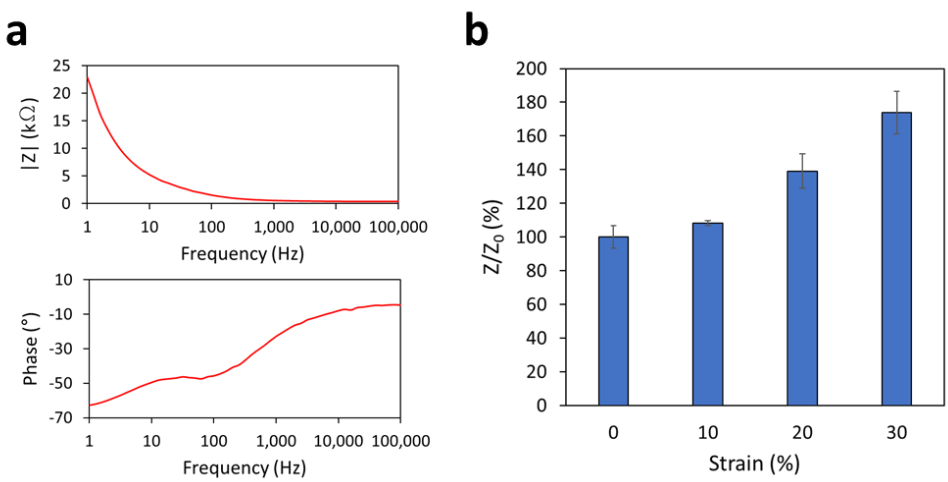

Figure 5. (a) The impedance and phase angle spectra of the in vivo epicardial signal recording bioelectronics, and (b) the variance of the impedance under mechanical strains up to 30% (n=3).

Among the various applications, we highlighted the potential of the bioelectronics produced by NW-SF to perform epicardial signal recording with dynamic movements of a rodent's heart. Epicardial signal recording is an emerging measurement method where flexible electrodes are arrayed and placed on the

heart's surface to monitor its spatial physiological conditions[7]. Before attempting the application, the impedance of the printed electrodes was measured to assess the signal measurement performance of the printed device. The obtained results (**Figure 5a**) and references from previous studies[8] suggest that the electrodes we fabricated are suitable for the use as cardiac implantable bio-signal electrodes. Additionally, impedance measurements were taken under stretching conditions, showing that at 30% strain with 1 kHz frequency, the impedance increased by less than 1.7 times (**Figure 5b**). This supports the conclusion that the electrodes are suitable for cardiac signal measurements.

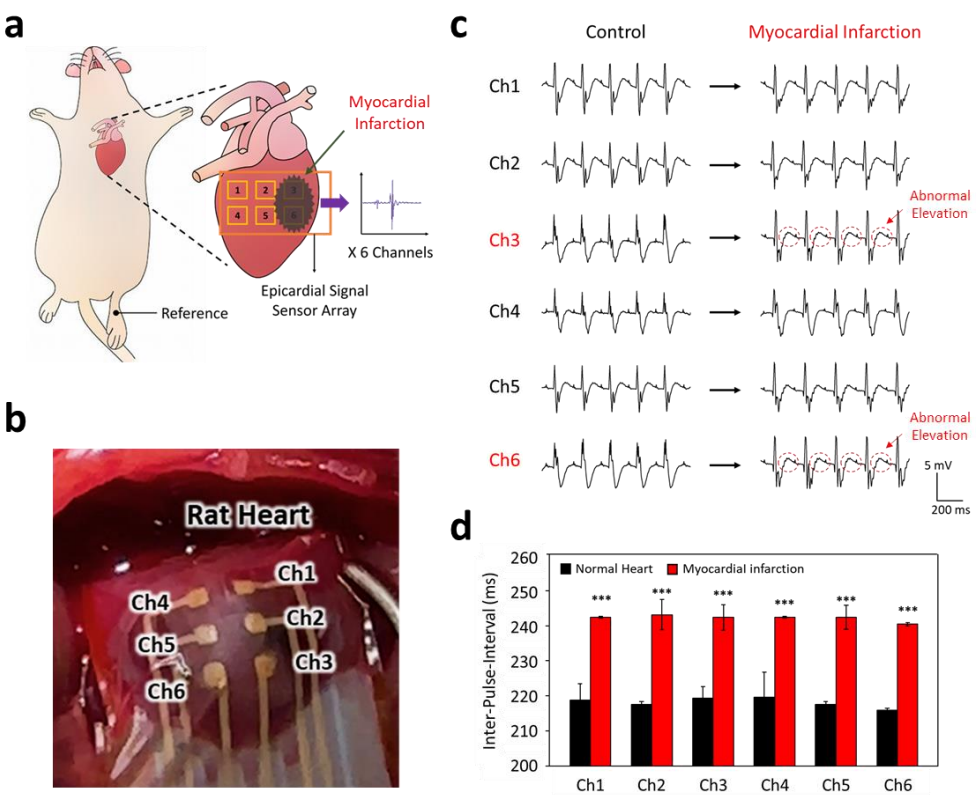

Figure 6. (a) The schematic diagram of the epicardial signal recording with the bioelectronics fabricated through NW-SF, (b) the enlarged image of the epicardial signal recording, (c) the result of the epicardial signal recording from a healty rat and a rat with myocardial infarction, and (d) the comparison of the inter-pulse-

interval between a rat with (w/) and without (w/o) myocardial infarction. (n=3)

In addition, the NW-SF process can effectively be applied to patterning small area electrodes of Ag@Au NW with high electrical conductivity and impedance. As a result, even on the small size of a rodent's heart, multiple electrodes can be effectively arranged in an array format to measure the changes of bio-signals from different heart locations through multiple channels (**Figure 6a, 6b**). (The size of a mouse heart is typically about 1 cm^2, and its strain is known to be approximately 30%[9].) Therefore, epicardial signal acquisition bioelectronics of appropriate sizes were fabricated through NW-SF, with the area of 1 mm^2 for each electrode, and a total of six electrodes were patterned to enable simultaneous spatial epicardial signal recording from different positions on the heart. When these electrodes were attached to a rat's heart to measure the signals, it was confirmed that all six electrodes provided effective epicardial signal recordings (**Figure 6c**).

Furthermore, to assess whether these electrodes could be harnessed to analyze the heart's physiological condition, the signals from a healthy rat's heart were compared with those from a rat's heart in a state of myocardial infarction. The result showed that sectional signals (Ch3, Ch6) exhibited abnormal elevation which is a resemblant symptom of myocardial infarction[7b], demonstrating the availability of our patterned bioelectronics to evaluate the physiological condition of the heart. Additionally, longer signal intervals were observed in all signals for the heart with myocardial infarction, and such phenomena are consistent with findings from previous research on myocardial infarction[10]. Therefore, it can be concluded that the signals decoded by the fabricated electrodes effectively captured the state of myocardial infarction of the heart. Consequently, it was confirmed that NW-SF

allows the fabrication of biocompatible electrodes that can function well even under conditions of significant mechanical deformation like heart beating.

Chapter 4. Non-enzymatic biosensor for ascorbic acid detection

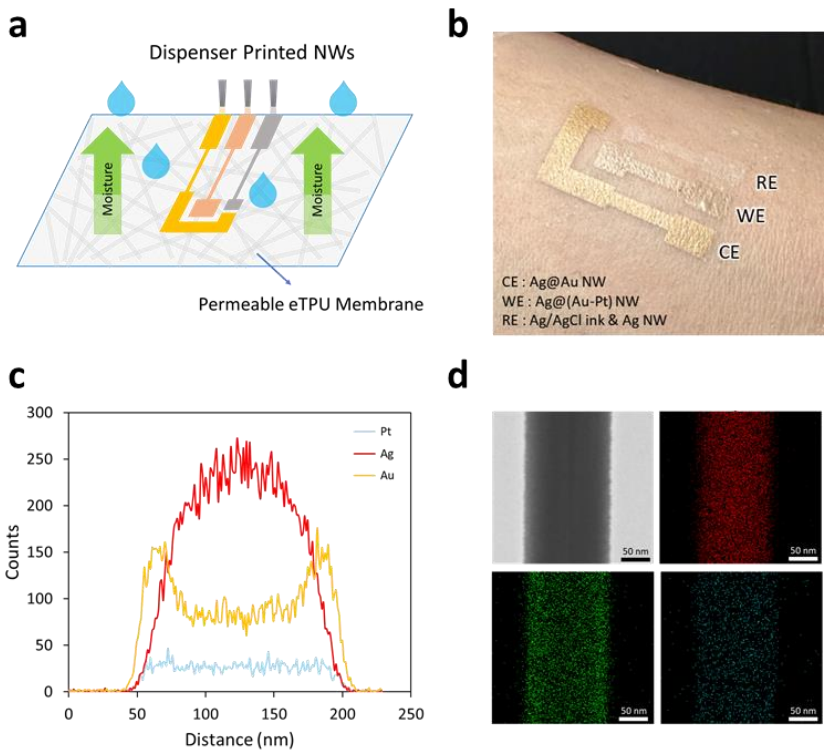

Figure 7. (a) The schematic image of a printed three-electrode biosensor and (b) skin-attached printed biosensor composed of three different sorts of nanowires fabricated by NW-SF. (c) Energy-dispersive X-ray spectroscopy (EDS) cross-sectional line scan plot and (d) mapping image (Red : Ag, Yellow : Au, Blue : Pt) of Ag@(Au-Pt) NW from transmission electron microscopy (TEM).

4.1. Fabrication of the non-enzymatic biosensor

Additional advantage of NW-SF is the availability of harnessing multiple nanomaterials in situ to fabricate flexible bioelectronics with advanced functionalities. Especially, there has been rarely introduced fiber-based electronics composed of multiple nanomaterials, because of the complexity of prevalent

fabrication processes. As a proof of concept, we fabricated a novel electrochemical biosensor with three-electrode system which was printed with different kinds of metal nanowires on fiber-based eTPU substrate (**Figure 7a, 7b**). Recently, research about Ag NW-based core-shell nanowire synthesis has been vigorously conducted, in order not only to maintain high electrical conductivity but also to integrate additional functionalities through the characteristic shells. In this research, Ag@Au and Ag@(Au-Pt) NW were synthesized for counter electrode (CE) and working electrode (WE) of the fabricated biosensor. Ag@Au NW is well known for its resistance of diverse redox reactions[11], which are suitable to consist CE to enable stable current measurement. Newly synthesized Ag@(Au-Pt) NW utilized its catalytic characteristics of Au-Pt alloy shell to detect ascorbic acid (AA) in body fluid. The synthesized core-shell nanowire's composition was analyzed by transmission electron microscope (TEM) (**Figure 7c, 7d**). Au-Pt alloy nanomaterials can work as enzyme-mimetic catalysts which can accelerate oxidation of AA to ascorbyl radical[12]. In this regard, we synthesized Ag@(Au-Pt) NW working similar to ascorbate oxidase to develop electrochemical biosensor evaluating the concentration of AA through amperometry analysis. For the reference electrode (RE), we utilized Ag nanowire and Ag/AgCl ink to maintain stabilized reference potential.

4.2. Electrochemical analysis for ascorbic acid detection

With the aim of finding proper voltage to conduct chronoamperometry, we firstly analyzed the current in voltage range of -0.09 V to 0.09 V with WE made of Ag@(Au-Pt) NWs. We could find that at 0.04 V, the current was measured as 68.4

μA in the solution of 600 μM AA with phosphate buffered saline (PBS) while there was mere current change (5 μA) in pure PBS (**Figure 8b**).

At the voltage that we found proper from cyclic voltammetry (0.04 V), we conducted chronoamperometry with biosensor we fabricated to detect AA in PBS with concentration up to 1,309 μM. As a result, we could ascertain that our fabricated biosensor can effectively detect AA concentration with sensitivity of 111.1 nA/μM with high linearity (R^2 = 0.9822) (**Figure 8c**).

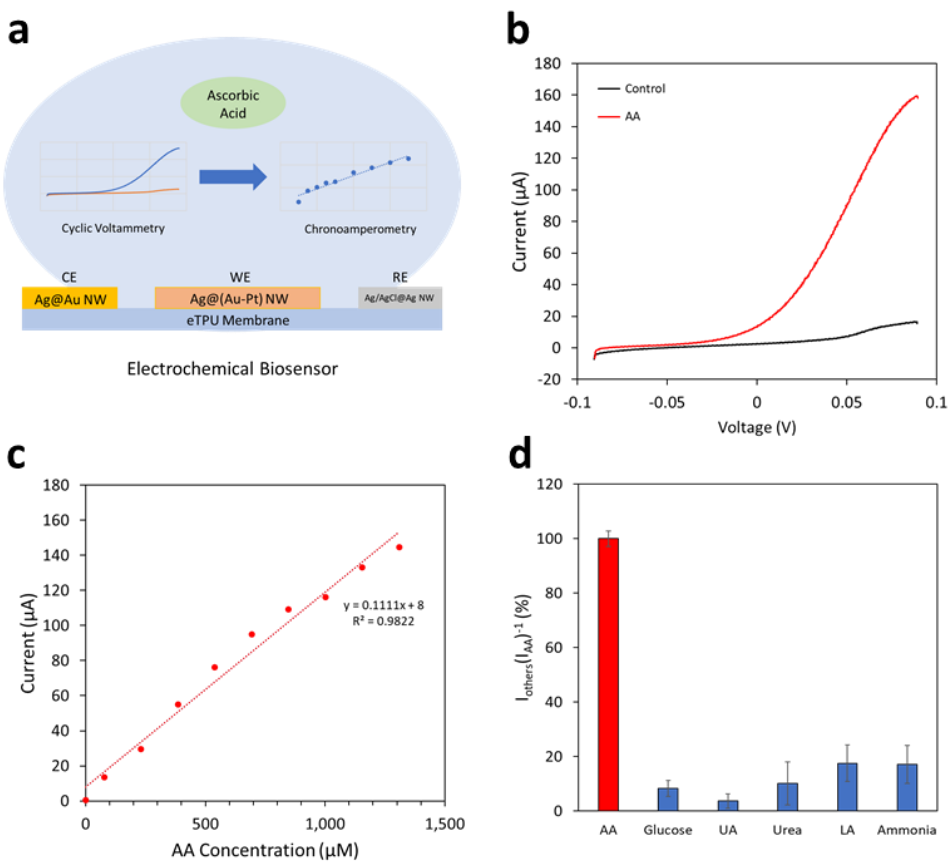

Figure 8. (a) The schematic image of the three-electrode biosensing principle, (b) cyclic voltammetry plot comparing cases w/ and w/o ascorbic acid in phosphate buffered saline (PBS) electrolyte, (c) sensitivity plot of printed biosensor with ascorbic acid concentration variation and (d) selectivity plot of printed biosensor with diverse components in body fluid.

Moreover, the selectivity of the fabricated biosensor was also analyzed quantitatively. Same amperometry method was implemented with extra five different materials (glucose, uric acid (UA), urea, lactic acid (LA), ammonia) that are prevalent in body fluid (concentration of all materials was 200 μM). The result showed that the current change from the materials were relatively low enough for the biosensor to detect AA (**Figure 8d**). AA biosensor has earned huge interests to track nutritional status in daily life, which can help manage dietary habits and nutrition consumption[13]. Specifically, non-invasive nutrition monitoring has tremendous potential for daily nutritional monitoring without discomfort. The biosensor we suggest can effectively absorb hydrous liquid through simple O_2 plasma treatment. Therefore, the biosensor fabricated through simple NW-SF is expected to be effectively utilized as a novel medium for facile daily nutrition management.

Chapter 5. Fabrication of Customized Human-Machine Interfaces (HMI)

5.1. Importance of the customized bioelectronics fabrication

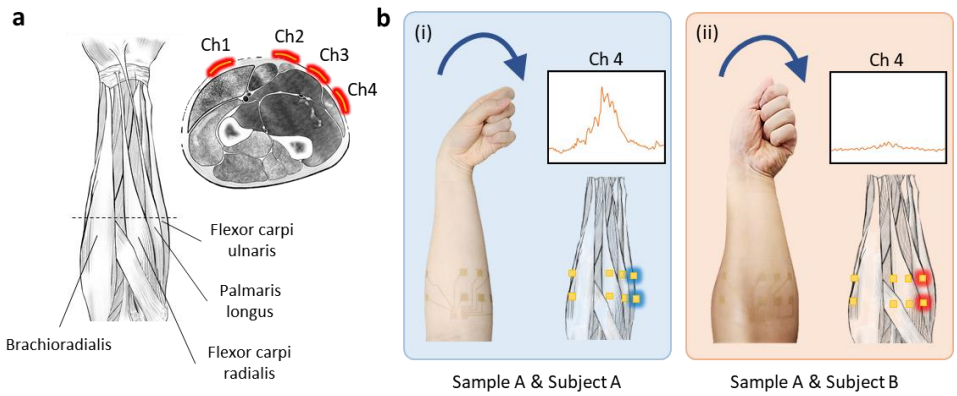

Figure 9. (a) The schematic diagrams of the anatomical structure of the forearm (left arm) and (b) comparison of the electromyography signals from two subjects who are w/ and w/o their customized bioelectronics.

NW-SF is also effective for swift design modification of customized flexible bioelectronics fabrication. Previous fabrication processes utilizing mask patterning of nanomaterials have had impediments to flexibly change their pattern design. Such hardship can induce critical problems in the field of bioelectronics fabrication. Because each person, including infants and amputees, has a different shape and size of their body part, it is difficult to manufacture individually, and functionally customized bioelectronic devices in the process of producing uniformly standardized design. Recently, several implementations to analyze proper positions for electrode placement have been continuously attempted to enhance the performance of the bioelectronics, including anatomical analysis[14],

electromyogram (EMG) mapping[14], and mechanical strain mapping[15]. The refined results from such research have demonstrated the importance of comprehending appropriate spots to attach electrodes of flexible bioelectronics. In this regard, here we corroborate the versatility of NW-SF to fabricate customized human-machine interface (HMI) bioelectronics which can classify hand gestures from EMG signals of individual's forearm. Our work harnessed anatomical information of forearm for the design of customized HMI fabrication. The major muscles functioning when we make hand gestures were selected for electrode placements, including Brachioradialis, Flexor carpi radialis, Palmaris longus, and Flexor carpi ulnaris (**Figure 9a**). According to the anatomical muscle arrangements, customized EMG-based HMI bioelectronics were fabricated through NW-SF for subject A and subject B, who have different size of the forearm. Then EMG signals were measured from subject A and subject B with customized HMI only for subject A. Comparing the signals from the two devices, we could ascertain that the two electronics showed different EMG signals from each other (**Figure 9b**). When the subject B utilized the bioelectronics bespoke for the subject A, the channel 4, which was designated to be attached on Flexor carpi ulnaris, was located on Palmaris lingus, whose signal is different from the former muscle. The amplitude and the overall form of the signals were different from each other. Moreover, the two probes of channel 2 are located on different muscles of subject B, which can induce improper acquisition of surface EMG signal. Therefore, we could conclude that swift customization of bioelectronics through NW-SF will be effective for HMI fabrication, which should accord with individual's body parts' characteristic shape. In order to evaluate the viability of the customized bioelectronics as HMI, we conducted a hand gesture classification with deep learning approach.

5.2. Hand gesture classification with deep learning approach

As hand gesture classification has been widely exploited as a medium for machine control through HMI, including robot manipulation[14], keyboard typing[6], computer manipulation[14] and virtual reality applications[6], we chose it as our performance evaluation strategy. For proper EMG signal acquisition, we carefully designed 4-channel EMG signal circuit and fabricated the bioelectronics through NW-SF. As a deep learning model, we implemented InceptionTime model[16] which has shown superior performance in time-series classification even with large dataset within short learning time (**Figure 10**). Total 5 gestures (Gesture 1 : Five, Gesture 2 : Little, Gesture 3 : Thumb, Gesture 4 : Right, Gesture 5 : Up) were utilized and 130 data were collected for each gesture. Train and test dataset were divided as 4:1 and trained for 40 epochs. As a result, we could successfully demonstrate that the customized EMG acquisition bioelectronics can classify 5 hand gestures with 96.15% (**Figure 11a, 11b**). The utilization of this HMI system with NW-SF process is expected to enable various HMI applications such as keyboard typing without touching and translation of hand signal language through the fabricated HMI bioelectronics. As a result, we could demonstrate that NW-SF has considerable potential in fabricating epidermal bioelectronics in order to reflect customized characteristics of each individuals.

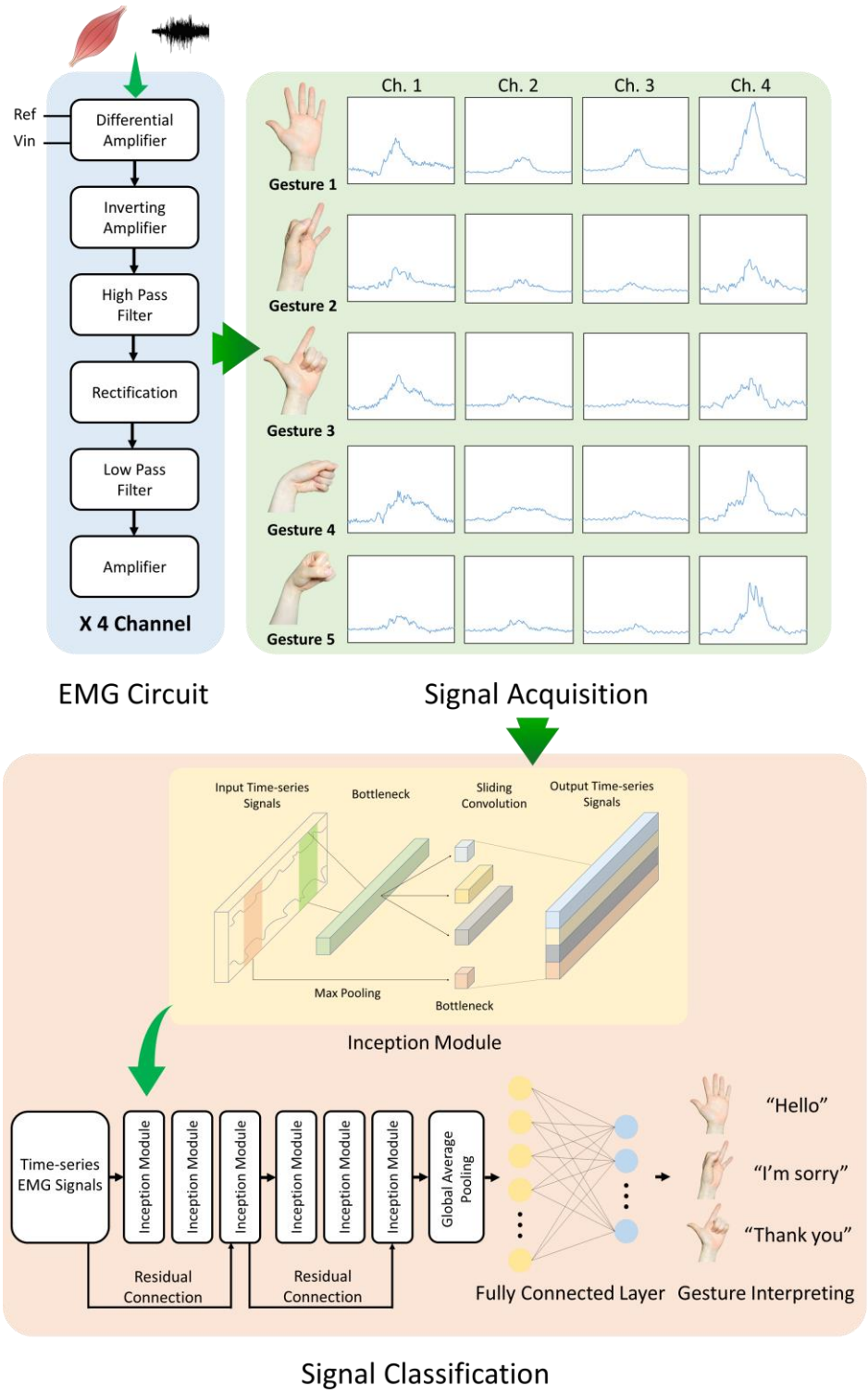

Figure 10. The schematic diagram of the overall structure of the hand gesture classification with customized human-machine interface (HMI) bioelectronics.

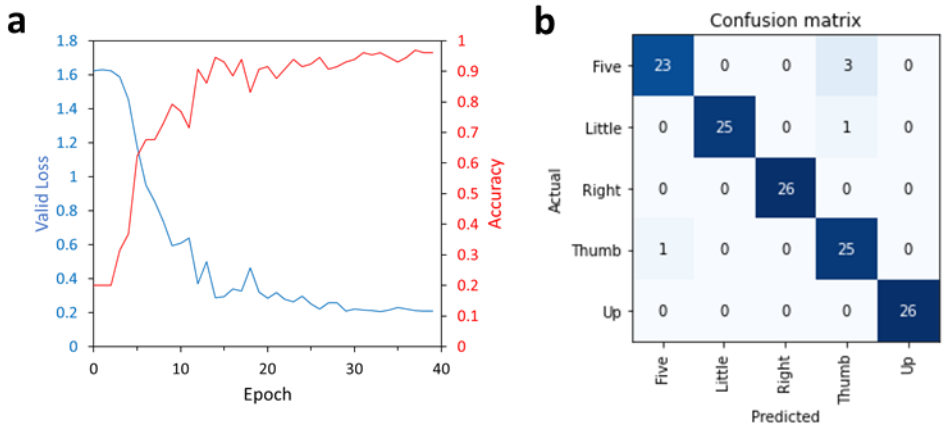

Figure 11. (a) The valid loss & the accuracy plot and (b) the confusion matrix of the result from the hand gesture classification with deep learning approach.

Chapter 6. Conclusion

In this research, we developed a novel method of metal nanowire patterning on porous electrospun fiber-based polymer membrane. Harnessing the liquid-absorbing characteristics of the supported carbon paper during the printing process, we could realize diverse resolution of printing by manipulating various parameters. Moreover, additional post laser process was implemented in order to improve robustness and stability of the patterned electronics. Patterned electronics fabricated through such process has high permeability and high electrical conductivity under strain, which endow high potential for them to be utilized as an epidermal, wearable bioelectronics. In this regard, we successfully suggested an in vivo epicardial electronics, an epidermal electrochemical biosensor and an epidermal human-machine interface. In conclusion, the developed nanowire printing method is expected to become a new medium for manufacturing diverse breathable skin electronics with high efficiency and effectiveness.

Chapter 7. Methods

7.1. Materials

Ethylene glycol (EG, 99.5%), Sodium hydroxide (NaOH, bead, 98%), Ammonia solution (NH_3, solution in water, 25.0-30.0%), Phosphate buffered saline (PBS, BP-PBS 10X solution), and n-Hexane (Hexane, 95.0%) were purchased from Samchun Chemical Co., Ltd. Silver(I) nitrate (AgNO3, 99.9%) and Chloroplatinic acid hydrate ($H_2PtCl_6 \cdot nH_2O$, 99.0%) were purchased from Kojima Co., Ltd. Polyvinylpyrrolidone (PVP, Mw = 360,000, Mw = 40,000), Copper(II) chloride dihydrate ($CuCl_2 \cdot 2H_2O$, 99.999%) Gold(III) chloride trihydrate ($HAuCl_4 \cdot 3H_2O$, ≥99.9% trace metals basis), Sodium sulfite (Na_2SO_3, ACS reagent, ≥98.0%), L-ascorbic acid (L-AA, ACS reagent, ≥99%), D-(+)-Glucose (ACS reagent), Urea (ACS reagent), Uric acid (≥99%, crystalline) and Lactic acid solution (ACS reagent, ≥85%) were purchased from Sigma Aldrich. Ag/AgCl ink was purchased from ALS-Japan.

7.2. Synthesis of the Ag nanowire (Ag NW)

AgNWs were synthesized utilizing a similar method from recent studies[17]. 3.182 g of PVP (Mw = 360,000) in 260 mL of EG was heated at 175°C (130 rpm). After it was properly heated, 1.6 mL of 4 mM $CuCl_2 \cdot 2H_2O$ was added. After 10 minutes, 60 mL of 100 mM $AgNO_3$ in EG is injected via a syringe pump with the rate of 3 mL min-1. After the injection, we stopped the stirring and allowed the synthesis reaction for 2 hours. AgNWs were diluted with 900ml of acetone and the residual

solution was removed to obtain aggregated NWs. Aggregated NWs were dispersed in distilled (DI) water and cleaned with centrifugation of 2,500 rpm for 5 min several times. Finally, the purified AgNWs solution is adjusted to a concentration of 16 mg mL-1.

7.3. Synthesis of Ag@Au core-shell nanowire (Ag@Au NW)

The Ag@Au NWs were synthesized by modifying strategies from recent studies[11]. The Au precursor solution was made with 30 mg of $HAuCl_4 \cdot 3H_2O$, 33 mg of NaOH, and 17 mg of Na_2SO_3 in 70ml of DI water. After 24 hours under 4℃, another solution was prepared with 800 mg with 70 mg of NaOH, 300 mg of L-AA, PVP (Mw 40,000), and 10 mg of Na_2SO_3 into 100 ml of Ag NW solution. Consequently, the Au precursor solution was mixed with as-repared Ag NW solution. After 120 minutes, the Au shell was epitaxially reduced on the Ag NWs. For the final step, the synthesized Ag@Au NW were cleaned multple times with DI water and harnessed by depositing them into ethanol solvent.

7.4. Synthesis of Ag@(Au-Pt) core-shell nanowire (Ag@(Au-Pt) NW)

The Ag@(Au-Pt) NWs were synthesized by similar method of Ag@Au NW. The (Au-Pt) growth solution was prepared by mixing 140 mg of $HAuCl_4 \cdot 3H_2O$, 110 mg of NaOH, and 132 mg of Na_2SO_3 in 40 ml of DI water. After mixing the solution, add 70 mg of $H_2PtCl_6 \cdot nH_2O$ in the solution. The solution was mixed with 240 ml of DI water and left undisturbed for 24 hours under 5 ℃. Another solution was prepared with 1.32 g of L-AA, and 44 mg of Na_2SO_3, 3.6 g of PVP (Mw 40,000),

280 mg of NaOH, and 15ml of Ag NW solution with 395 ml of DI water. After all, the (Au-Pt) growth solution was softly poured into the Ag NW solution. After 120 minutes, the (Au-Pt) alloy shell was epitaxially reduced on the Ag NWs. For the final step, the synthesized Ag@(Au-Pt) NW were cleaned multple times with DI water and harnessed by depositing them into ethanol solvent.

7.5. Material characterizations

Scanning electron microscopy (SEM) images were characterized by Field-Emission SEM (MERLIN Compact; Carl Zeiss). Transmission electron microscopy (TEM) images were characterized by Analytical TEM (JEM-2100F; JEOL) and Energy Dispersive Spectroscopy (EDS) analysis was conducted to obtain the spatial distribution of elements of the samples. Fourier-transform infrared spectroscopy (FT-IR, Spectrum Paragon; PerkinElmer) was utilized to obtain radiation absorbance characteristics of the samples. A tensile stress measurement was conducted with a universal testing machine (UTM, Instron-5543; Instron). The electromechanical performance test was conducted with a uniaxial tensile load system (Physik Instrumente) and the real-time data was achieved by the PXIE hardware system with LabVIEW software (National Instrument).

7.6. Laser specification

The laser nanowire-embedding process was conducted by the continuous wave laser with a wavelength of 532 nm (Sprout-G-5 W; Lighthouse Photonics). The beam was ejected with raster scan mode following hatch design with 0.5 mm interval. The power range for NW-SF was between 80-100 mW with the laser

scanning speed of 40 mm/s operated by Galvano mirror scanner (hurrySCAN II; Scanlab).

7.7. Electrochemical analysis

All electrochemical analyses were conducted with an electrochemical workstation (VersaSTAT 3; Princeton Applied Research). Impedance and phase of the epicardial signal recording bioelectronics were evaluated by potential electrochemical impedance spectroscopy (EIS) with three-electrode system, consisting of Ag@Au NW electrode (1mm*1mm) printed with NW-SF as a working electrode (WE), Pt mesh counter electrode (CE), and Ag/AgCl reference electrode (RE) with 5mV root mean square (RMS) in PBS. The impedance variance under mechanical strains were analyzed at 1 kHz. Cyclic voltammetry of the non-enzymatic biosensor was also conducted with three-electrode system, consisting of Ag@(Au-Pt) NW electrode of the biosensor printed with NW-SF as a working electrode (WE), Pt mesh counter electrode (CE), and Ag/AgCl reference electrode (RE). Chronoamperometry was conducted with three-electrode system composing the biosensor and the first current was plotted from the chronoamperometry whose interval was 1 second. Selectivity of the biosensor was evaluated by same chronoamperometry setup with various substances in PBS.

7.8. Electromyography (EMG) signal acquisition circuit

The basic backbone of our EMG circuit is inspired by H.M. Desa et al.[18]. For each channel, two probes work as an EMG signal sensor, and 4 channels were utilized to acquire EMG signals from different body parts. For the electrode, the

EMG signal acquisition bioelectronics fabricated by NW-SF was adopted, which was attached on the forearm with a small amount of conductive gel (Tensive conductive adhesive gel; Parker). EMG signal passed through the first differential Amplifier. We used INA 106 (Texas Instruments) to amplify signal differences between probe 1 and 2 which can also cancel ambient noises. Harnessing 1 MΩ external resistor as a feedback resistor, the gain value was set as 110. The virtual ground of INA106 works as a reference, which is connected to an elbow joint of the human body. To produce 180° phase shift with amplifying, the signal was passing inverting amplifier, and the inverted signal difference amplified with the gain of 15 according to our resistor arrangement. The signal from the inverting amplifier goes through an active high pass filter (HPF), which can make the cutoff frequency. As we used 150 kΩ resistor 10 nF capacitor, we could get 106 Hz of cutoff frequency. After regulating from HPF, full wave rectifier flips the negative voltage signal to make it all-positive. This could make voltage variance into half, and make us more comfortable to take analysis of the signal. Another filtering step is using low pass filter (LPF) to eliminate the aliasing effect. As we use 82 kΩ resistor and 1 μF capacitor, the cutoff frequency of LPF is 2 Hz. Finally, we arranged final amplifier using 100 kΩ trimmer, which can make us to control the amplitude of the output.

For the microprocessor, we used CC2640R2F (Texas Instruments) and signal acquisition code was composed with Code composer studio IDE (CCSTUDIO IDE; Texas Instruments).

Reference

[1] D.-H. Kim, N. Lu, R. Ma, Y.-S. Kim, R.-H. Kim, S. Wang, J. Wu, S. M. Won, H. Tao, A. Islam, *Science* **2011**, 333, 838.

[2] Y. Wang, T. Yokota, T. Someya, *NPG Asia Materials* **2021**, 13, 22.

[3] Z. Jiang, M. O. G. Nayeem, K. Fukuda, S. Ding, H. Jin, T. Yokota, D. Inoue, D. Hashizume, T. Someya, *Advanced Materials* **2019**, 31, 1903446.

[4] T. Y. Suman, D.-S. Pei, in *Nanomaterials Recycling*, Elsevier, 2022.

[5] C. T. McKee, J. A. Last, P. Russell, C. J. Murphy, *Tissue Engineering Part B: Reviews* **2011**, 17, 155.

[6] K. K. Kim, M. Kim, K. Pyun, J. Kim, J. Min, S. Koh, S. E. Root, J. Kim, B.-N. T. Nguyen, Y. Nishio, *Nature Electronics* **2023**, 6, 64.

[7] a)K. Sim, F. Ershad, Y. Zhang, P. Yang, H. Shim, Z. Rao, Y. Lu, A. Thukral, A. Elgalad, Y. Xi, *Nature Electronics* **2020**, 3, 775; b)B. Kim, A. H. Soepriatna, W. Park, H. Moon, A. Cox, J. Zhao, N. S. Gupta, C. H. Park, K. Kim, Y. Jeon, *Nature Communications* **2021**, 12, 3710.

[8] a)J. Zhu, S. Yang, Y. Qi, Z. Gong, H. Zhang, K. Liang, P. Shen, Y.-Y. Huang, Z. Zhang, W. Ye, *Science Advances* **2022**, 8, eabk0011; b)Z. Chen, K. Nguyen, G. Kowalik, X. Shi, J. Tian, M. Doshi, B. R. Alber, X. Guan, X. Liu, X. Ning, *Advanced Materials Technologies* **2023**, 2201716.

[9] J. Park, S. Choi, A. H. Janardhan, S.-Y. Lee, S. Raut, J. Soares, K. Shin, S. Yang, C. Lee, K.-W. Kang, *Science translational medicine* **2016**, 8, 344ra86.

[10] S.-H. Sunwoo, M.-J. Cha, S. I. Han, H. Kang, Y. S. Cho, D.-H. Yeom, C. S. Park, N. K. Park, S. W. Choi, S. J. Kim, *Science advances* **2023**, 9, eadf6856.

[11] S. Choi, S. I. Han, D. Jung, H. J. Hwang, C. Lim, S. Bae, O. K. Park, C.

M. Tschabrunn, M. Lee, S. Y. Bae, *Nature nanotechnology* **2018**, 13, 1048.

[12] a)W. He, X. Han, H. Jia, J. Cai, Y. Zhou, Z. Zheng, *Scientific reports* **2017**, 7, 40103; b)Y.-T. Zhou, W. He, W. G. Wamer, X. Hu, X. Wu, Y. M. Lo, J.-J. Yin, *Nanoscale* **2013**, 5, 1583.

[13] J. R. Sempionatto, A. A. Khorshed, A. Ahmed, A. N. De Loyola e Silva, A. Barfidokht, L. Yin, K. Y. Goud, M. A. Mohamed, E. Bailey, J. May, *ACS sensors* **2020**, 5, 1804.

[14] Y.-T. Kwon, Y.-S. Kim, S. Kwon, M. Mahmood, H.-R. Lim, S.-W. Park, S.-O. Kang, J. J. Choi, R. Herbert, Y. C. Jang, *Nature communications* **2020**, 11, 3450.

[15] T. Sun, F. Tasnim, R. T. McIntosh, N. Amiri, D. Solav, M. T. Anbarani, D. Sadat, L. Zhang, Y. Gu, M. A. Karami, *Nature biomedical engineering* **2020**, 4, 954.

[16] H. Ismail Fawaz, B. Lucas, G. Forestier, C. Pelletier, D. F. Schmidt, J. Weber, G. I. Webb, L. Idoumghar, P.-A. Muller, F. Petitjean, *Data Mining and Knowledge Discovery* **2020**, 34, 1936.

[17] L. J. Andrés, M. F. Menéndez, D. Gómez, A. L. Martínez, N. Bristow, J. P. Kettle, A. Menéndez, B. Ruiz, *Nanotechnology* **2015**, 26, 265201.

[18] H. Desa, M. Zuber, R. Jailani, N. Tahir, presented at *2016 IEEE Symposium on Computer Applications & Industrial Electronics (ISCAIE)*, **2016**.

국문 초록

유연 생체전자기기 제작을 위한 통기성 섬유 기판 기반 금속 나노와이어 패터닝 연구

윤혁준
기계공학부
서울대학교 대학원

최근 들어, 폴리머 섬유 기반 유연 기판은 통기성과 신축성, 생체적합성으로 인해 생체전자기기의 기판으로 큰 주목을 받아왔다. 본 연구에서는, 다양한 전도성 금속 나노와이어를 폴리머 섬유 기반 유연 기판에 신속하고 정밀하게 패터닝함으로써 효과적으로 유연 생체 전자기기를 제작할 수 있는 공정을 개발하였다. 나노 물질로는 은, 은@금, 은@(금-백금 합금) 코어-쉘 나노와이어를 합성하여 사용하였으며, 추가적인 레이저 공정을 통해 기계적, 전기적 안정성을 향상시킬 수 있었다. 또한 목적에 맞게 절연 물질을 프린팅하여 원하는 기능을 효과적으로 구현할 수 있도록 공정을 설계하였다. 이를 활용하여, 심장 부착형 심장 표면 신호 측정 생체전자기기, 피부 부착형 비타민 농도 측정 바이오 센서, 그리고 피부 부착형 근전도 기반 손동작 인식 인간-기계 인터페이스를 제작하여 그 성능을 검증함으로써, 본 연구에서 개발한 공정이 유연 생체전자기기 제작에 효과적으로 활용될 수 있음을 보여주었다.

주요어 : 유연 전자기기, 생체전자기기, 나노물질 패터닝, 나노물질 합성, 웨어러블 전자기기

학 번 : 2021-24389